Experimental and numerical analysis of the aerodynamics of peregrine falcons during stoop flight

C. Lagemann[1], E. R. Gowree[2], C. Jagadeesh[2], E. Talboys[2] and C. Brücker[2]
[1]Institute of Aerodynamics, RWTH Aachen University, Aachen, Germany
[2]Dept. Mechanics and Aeronautics, City University of London, London, UK
c.lagemann@aia.rwth-aachen.de

Abstract

Amongst birds, peregrine falcons (Falco peregrinus) are well-known for their unique high-speeds during stoop. A combination of time-resolved stereoscopic particle-image velocimetry (TR-SPIV), surface oil flow visualization (SOFV) and large-eddy simulations (LES) is used to analyze the complex flow over life-size models of peregrine falcons. It is demonstrated that the exceptional manoeuvrability of peregrine falcons during stoop is attributed to vortex dominated flow promoted by their morphology and their wing shapes. Both, experiments and simulations, revealed the presence of vortices emanating from the neck and the dorsal region due to a strong spanwise flow enhancing mixing for a quick reattachment to ensure a fully attached flow over the tail feather. The stronger wing and tail vortices further provide vortex induced lift for pitch and roll control.

1. INTRODUCTION

Peregrine falcons (Falco peregrinus) are very famous for high-speed stoops and theoretically are thought to reach velocities of more than 70 m/s [19]. Hunting prey at presumably the highest speed amongst animals on earth demands special aerodynamic, physiological and cognitive skills. A robust musculo-skeletal structure and feather of superior mechanical strength compared to other avians enable peregrine falcons to withstand the enormous forces during stoop [15]. Furthermore, the success of an attack also depends on the manoeuvrability which is closely related to special aerodynamic flow features [5]. When nose-diving from high altitude, peregrine falcons can repeatedly be seen morphing their wings intuitively. Within the initial phase of the stoop, peregrine falcons fold their wings around the body to adopt the lowest drag configuration called teardrop shape (T-shape). In C-shape, the falcon untucks its forearms slightly forming a small cavity between body and primary feathers. During M-shape, the wings open up furthermore into the horizontal plane while the primary feathers are aligned in freestream direction. Due to the gap between tail and primary feathers, this configuration resembles a 'M'-like shape when viewed from top. Different live recordings ([1], [8], [9]) confirmed the biological correctness of these wing shapes. Considering the high speeds achieved during such stoop manoeuvres, it appears that peregrine falcons have mastered these morphological transformations to manipulate the flow for improved aerobatics. To understand the basic flow phenomenon enabling peregrine falcons to perform such complex flight manoeuvres different series of wind tunnel testing have been conducted on life-size models. First, surface oil flow visualizations were used to capture the near-wall flow topology and to analyze the surface streamlines. Time-resolved stereoscopic particle-image velocimetry (TR-SPIV) was employed to gather more information about the evolution of vortical structures in the wake. Complementary large-eddy simulations confirmed the experimental findings and provided further details in regions where experiments were not possible.

2. EXPERIMENTAL AND NUMERICAL SETUP

The wing shapes of the different life-size models were obtained by 3D scanning a stuffed peregrine falcon fixing its wings with the morphology observed from detailed analysis of the high-speed optical tracking during field experiments [13]. The resulting surface data was prost-processed and the final life-size model was manufactured using rapid prototyping (3D printing). The chord length of the life-size models measures approximately 0.40 m while the individual span differs from 0.18 m (C-shape) to 0.23 m (M-shape).

According to [13], the aerodynamic reference of all measurements was set to a freestream velocity of 22.5 m/s which equals the maximum dive speed during the field experiments corresponding to a Reynolds number of approximately 5.8e+05. The angle of incidence of $\alpha = 5°$ was determined for an equilibrium flight condition and is defined as the angle between the chord line and the freestream direction (see Fig. 1). In free flight, it refers to the trajectory of the bird.

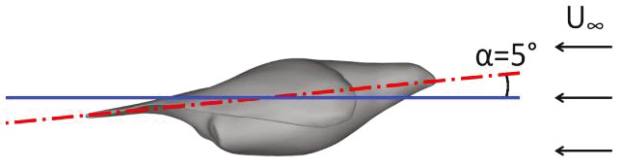

Figure 1. The angle of incidence is defined as the angle α between chord line and freestream direction.

The TR-SPIV experiments were conducted in the Handley Page Aeronautics Laboratory at City, University of London. The low speed wind tunnel facility provides flows ranging from 10 m/s to 45 m/s at moderate turbulence intensity lower than 1% and its test section measures 1.1 x 0.8 x 1.8 m. The falcon models were mounted on a sting and were placed in the center of the freestream. The crosssectional blockage amounts in less than 5 % and thus can be regarded as negligible. The TR-SPIV setup comprises of two Phantom Miro M310 (Vision Research)

doi:10.25967/480311

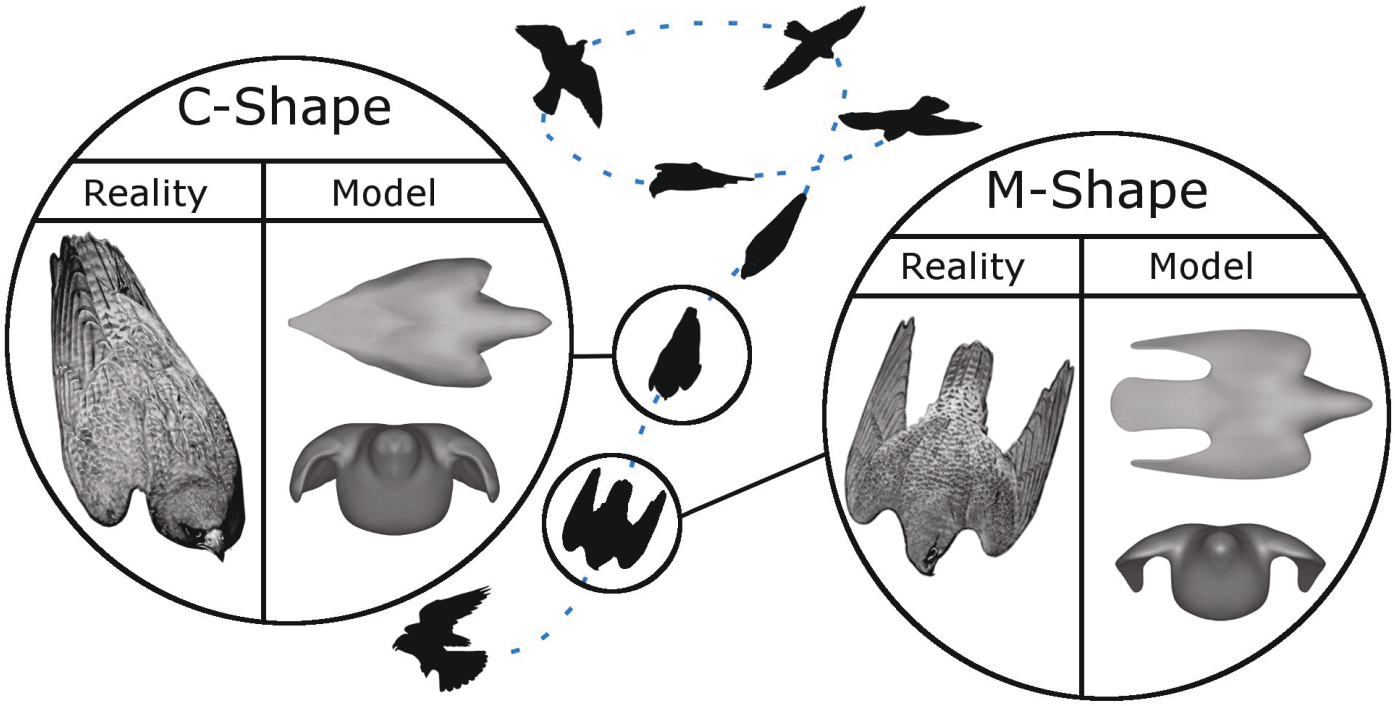

Figure 2. Falcon stoop montage showing typical wing configurations during an attack: While soaring in high altitude, the wings are completely stretched (see loop). During the first stage of an attack, peregrines adopt the T-shape. This configuration is replaced by the C- and M-shape which can be observed multiple times during stoop. Finally, the falcon decelerates rapidly attacking its prey.

and a Litron LDY303 double-pulsed laser expanded to a light sheet of 4 mm thickness as shown in Fig. 3. The PIV cameras were arranged in Scheimpflug condition (Scheimpflug angle β = 6°) and acquired particle images at a frame rate of 250 fps resulting in a frequency of f_{PIV} = 250 Hz. Each camera was equipped with a macro lens (Tokina 100 mm f/2.8) and its viewing angle was approximately θ/2 = 40°. Previous to the measurements, the air inside the wind tunnel facility was seeded with olive oil droplets with an averages size d_p = 1 µm. The particle image pairs were postprocessed with TSI 4G software

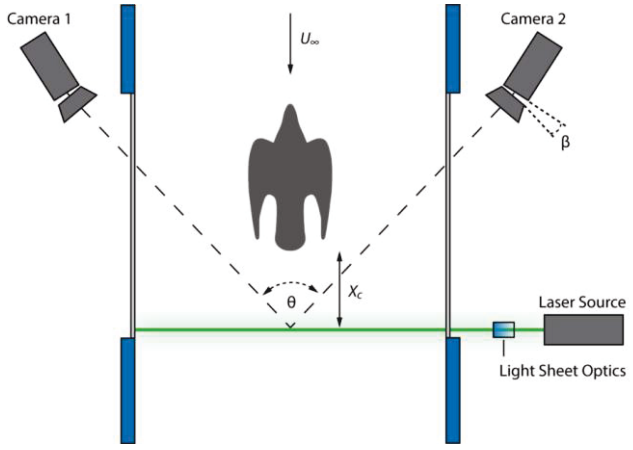

Figure 3. Overview of the TR-SPIV setup

using an adaptive cross-correlation with window shifting and deformation schemes. A decreasing multi-pass algorithm was applied leading to a final window size of 32 x 32 pixels with an overlap of 50%. In each test run a dataset of 1000 images was acquired. Prior to the evaluation, the images of each camera were dewarped using the calibration information of a four-plane target placed at the same position as the light sheet plane. The perspective mapping algorithm is based on the approach described in [16]. Due to a misalignment of the calibration target with respect to the laser light sheet, a certain error is automatically introduced in the reconstruction of the third velocity component. This error can be corrected by determining the local misalignment. Applying auto-calibration reconstruction based on [3] improves mapping so that the final reconstruction error is minimized. A universal outlier detection and a 3x3 local mean filter were applied to the calculated vector field to detect spurious vectors. The amount of spurious vectors was less than 2% of the entire vector dataset. For each life-size model, four different measurements planes were considered in the wake, 0.2c, 0.5c, 0.7c, and 1.0c downstream of the model where c equals the chord length.

The near-surface flow pattern on the falcon model is expected to be highly three-dimensional, especially with the appearance of local boundary layer separations. A visualization of the local skin friction is very helpful in studying and interpreting the complex interaction of flow phenomena close to the surface. The surface oil flow visualization (SOFV) was applied to visualize wall shear stress patterns and to detect local regions of separated boundary flow. The oil mixture comprised of white spirit (Naphta), luminescent powder (DayGlo) and Oleic acid and was applied using a fine bristled paint brush, right

before the tunnel was operated. With the wind tunnel running, the oil film is transported while dry pigments form a streaky pattern indicating the path of the surface flow and thus, the direction of the local skin friction vector. The evolution of the oil film was recorded and the final fully developed pattern was photographed under ultraviolet lighting to increase definition. Using the critical point theory, the topological representation of these near-surface streamlines helped in identifying and interpreting regions of detached flow and origins of vortices.

All numerical simulations were conducted using the commercial computational fluid dynamics code STAR CCM+ v.12 which is capable of doing steady and unsteady Reynolds-Averaged-Navier-Stokes (RANS) and large-eddy simulations (LES). The code numerically solves the conservation equations of mass and momentum using a finite volume approach. The chord length (c =0.4 m) based Reynolds number corresponds to Re = 5.8e+05 for a freestream velocity of 22.5 m/s. Therefore, turbulent flow is modelled using a Reynolds averaged and a large eddy approach. In case of RANS simulations, a two equation k – ω SST turbulence model is used and for the LES a Wall-Adapting Local-Eddy Viscosity (WALE) subgrid scale model is applied to model the turbulent viscosity μ_t.
The computational domain is decomposed in near-surface prism layers and a global Cartesian grid including two refinement zones. The initial mesh was based on a hexahedral trimmed mesh and had approximately 57 million cell for the M-shape and 63 million for the C-shape. The minimum grid spacing is based on $y^+<<1$ to resolve the fine scales in the boundary layer [10]. A second-order accurate scheme was selected for the temporal and spatial discretisation.The initial RANS simulations were regarded as converged when the residual of momentum (X,Y,Z) and the energy dropped below $\varepsilon = 10^{-5}$ which was always reached within 15 000 iteration steps. Each LES contains a corresponding physical time of 1 second using a timestep of $\Delta t = 10^{-5}$. The stability of the simulations was investigated with respect to different grid parameters (smaller/coarser grid).

Additionally, a smaller timestep was taken into account to neglect timestep induced errors. An example of the results of one such analysis on the numerical stability can be found in Fig. 4 showing the pressure distribution along the surface for all LES for the C-shape.

3. RESULTS

In the following, numerical and experimental results obtained from the simulations and the wind tunnel measurements will be presented. It is obvious that these investigations quantitatively cannot be of general nature regarding real flight cases, but are useful to gather a general understanding of the phenomenon also providing a reference case for comparison with avian species.
Furthermore, LES data provide more details which might not be interpreted in SOFV. To name one example, the singular points which can be analyzed using the critical point theory (CPT) [4], [6], [11], [18] are more pronounced and consequently can be identified more easily.

3.1. Flow topology of M- and C-shape

Due to the streamlined shape of the falcon's body and the unmatched flight performance during dive, one could be seduced to believe that the aerodynamic characteristics and the lift generation are similar to the ones already known from conventional airfoils, optimized for low drag and thus, promoting high-speed performance. However, the stoop flight is strongly influenced by several different vortex structures. In nature, the concept of unconventional lift generation, e.g. vortex induced lift generation [5], is widely spread and can be observed for flight of butterflies [2] & [17] or swifts [20]. Typically, the observed flow structures are highly three-dimensional and usually are based on flapping or due the complex morphology. As a result, this unconventional lift generation cannot be explained applying classical aerodynamic theories like the lifting-line theory. The complexity of the flow can already be guessed by analyzing the near-wall flow visualized in SOFV experiments and by constrained streamlines of LES. The detailed comparison between SOFV, LES and RANS simulations is shown in Fig. 6 .

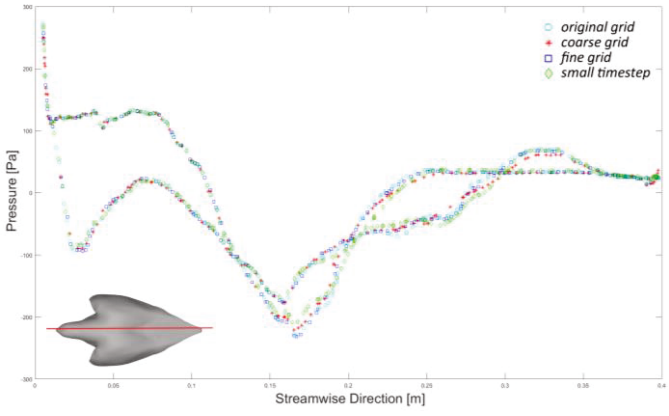

Figure 4. Results of the LES validation for the cupped wings: The reference case is highlighted in circles. The results of a coarser and finer grid are represented in red stars respectively blue squares while the results of the smaller timestep are represented in green diamonds.

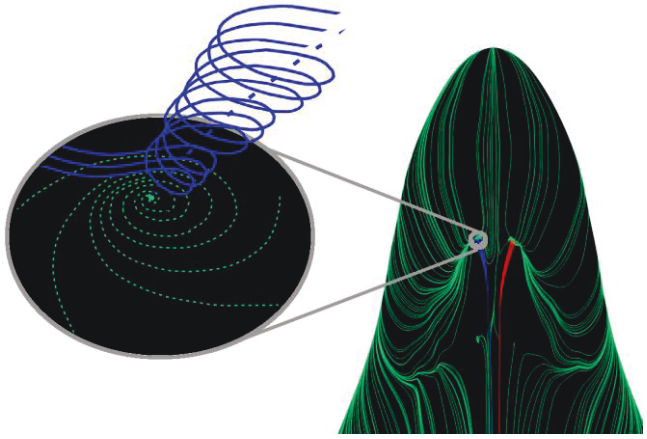

Figure 5. Formation of the horn vortex on the neck of the M-shape. The zoom on the left side shows a sketch illustrating the tornado-like vortex shape of the horn vortices.

Beginning near the nose, a detachment line (DL1) and a reattachment line (RL1) is visible surrounding two nodes. Using CPT, the nodes can be identified as the origin of two tornado-like vortices counter-rotating to each other. These vortices are similar to 'Werlé-Legendre' vortices present on slender cylindrical bodies at higher angle of attack [4] and consequently will be called horn vortices.

A detailed sketch and a streamline image are shown in Fig. 5. The junction between neck and forward swept wing facilitates the formation of another vortex. The singularities equal the critical point pattern of the flow around an obstacle perpendicular to the surface. First, the incoming flow separates in front of the wing along the primary separation line (S1) passing though the saddle

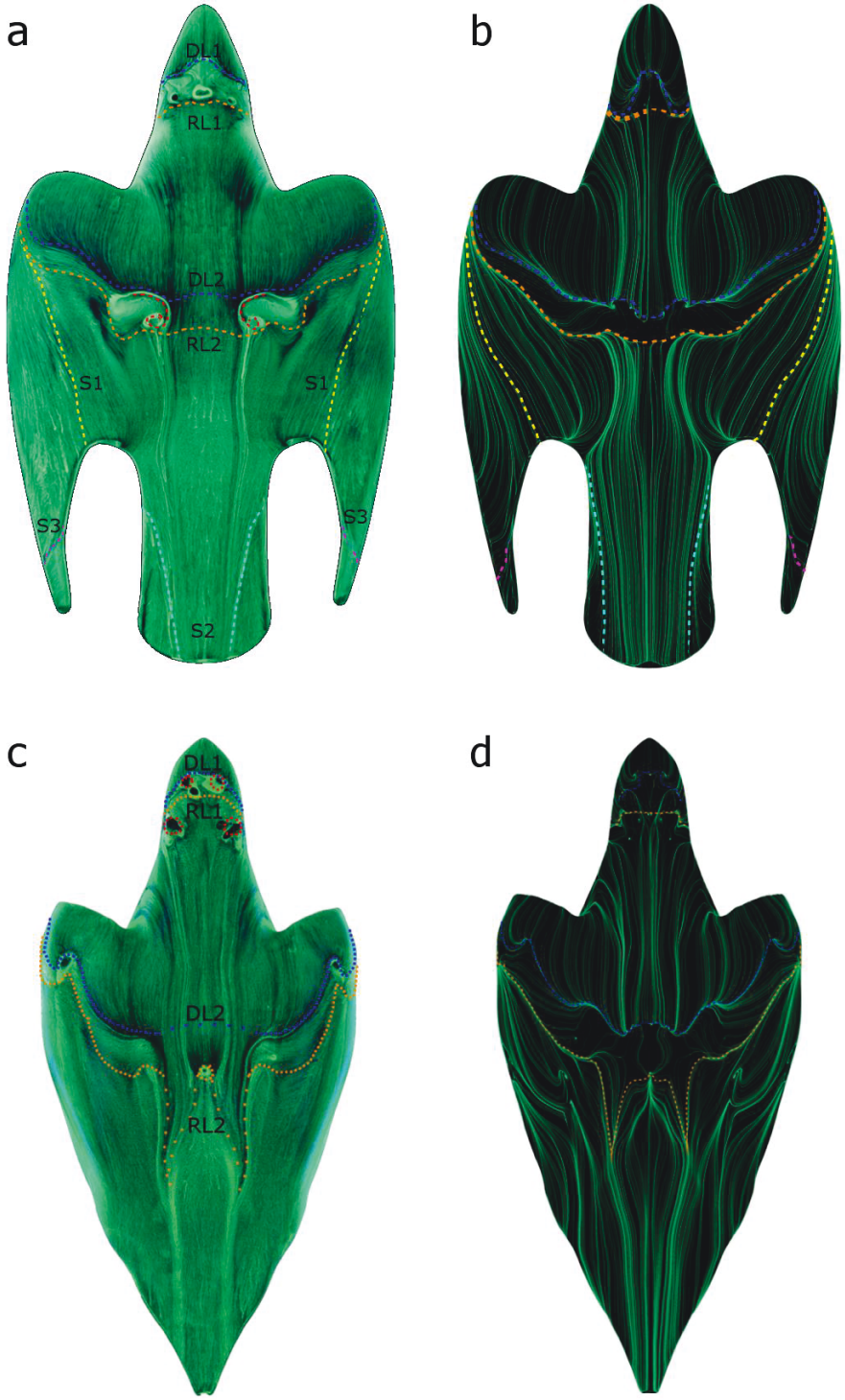

Figure 6. Experimental and numerical near-wall flow visualization of both wing configurations: a ,b M-shape, c,d: C-shape (from [5])

point S1. The flow emanating from (S1) rolls up to create a horse shoe vortex having a three-dimensional focus in its center. Shortly behind (S1), a nodal point of attachment becomes visible feeding the flow behind the first separation line. Slightly more downstream, the second separation line (S2) and its saddle point occur complementing the characteristic topology of a horse shoe vortex as described in [18]. A sketch of this flow topology is shown in Fig. 7 a. In comparison, Fig. 7 b shows the surface streamlines obtained by the large-eddy simulation of the M-shape. Since forward swept wings can be seen in both wing configurations, it is not surprising that one can see footprints of horseshoe vortices in the SOFV and LES images of Fig. 6 for both shapes.

Further downstream, on the outboard region of the leading edge the streamlines start to curl inboard forming a significant strong spanwise flow (approx. 15 – 20 % of freestream velocity) [5]. This spanwise flow is mainly based on an adverse pressure gradient caused by the highly curved 3D surface imposed by the musculo-skeletal structure. As visible in Fig. 8 the abrupt reduction of the wall shear stress indicates the formation of a weak recirculation area surrounded by detachment (DL2) and reattachment lines (RL2). The strong spanwise flow feeds the separation bubble and blows high momentum fluid to the inner dorsal region re-energizing the local boundary layer. A scenario which is similar to that of two opposite blowing jets promoting re-attachment of the flow. This flow separation control technique was demonstrated by Prandtl, where entrainment of higher streamwise momentum fluid is enhanced by the artificial injection of two jets [14]. The presence of the spanwise flow and the recirculation area is not only related to pure aerodynamic boundary layer re-energisation. In addition, this area has a huge impact on the natural flight control feedback loop system of peregrine falcons. As shown in [13], the feathers in this region are significantly smaller and thus can vibrate with a flow related frequency. These vibrations are transmitted to the distal of the feathers allowing peregrines to 'sense' the instantaneous flow condition.

Following the spanwise streamlines further inboard, the crossflow starts curling rapidly and ends up in a vortex similar to the horn vortex which is called dorsal vortex. Interestingly, the formation of the dorsal vortex can exclusively be seen in M-shape. This particular difference between C- and M-shape can be explained by the fact that the spanwise flow in case of M-shape exhibits an angle of approximately 80° with respect to the freestream direction while the angle of the crossflow angle of the C-shape is much smaller (approx. 60°). Thus, the spanwise velocity component is significantly higher in M-shape and promotes the formation of the dorsal vortex.

Other regions of highly curved streamlines can be found in the outboard region of the wing corresponding to a low wall-shear stress region in LES data (see Fig. 8). This region indicates a fairly strong vortex, called wing vortex, which is confirmed by the presence of the highlighted separation line S1 in Fig. 6. These vortices are generated at the tip of lifting surfaces where fluid flows from the high-pressure side to the low-pressure side. A similar phenomenon can be observed in the outer regions of the tail feathers. In case of the M-shaped wing configuration,

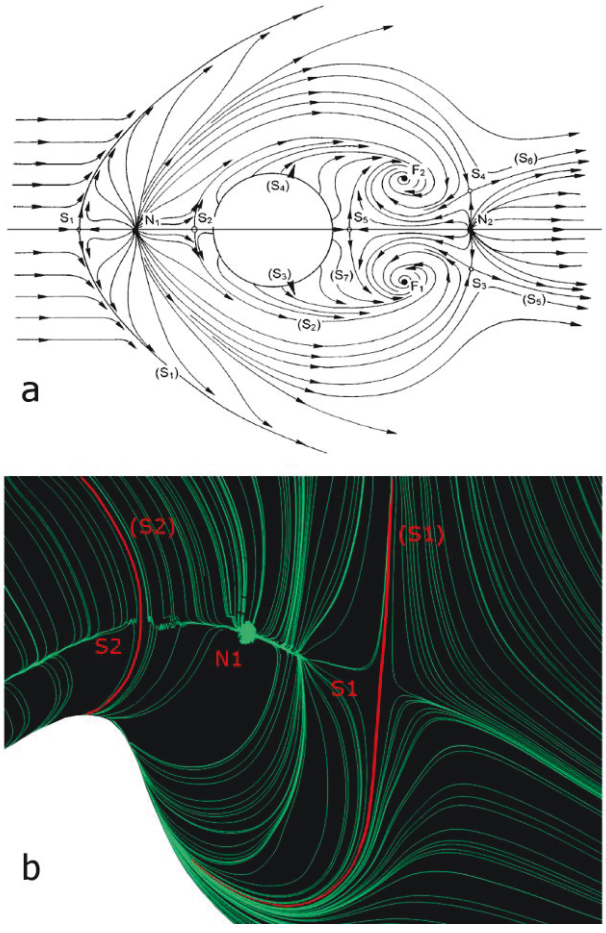

Figure 7. Formation of the horseshoe vortex in the junction neck and forward swept wing. a: Sketch illustrating the critical point pattern of a horseshoe vortex (from [4]), b: corresponding arrangement of singularities obtained by LES

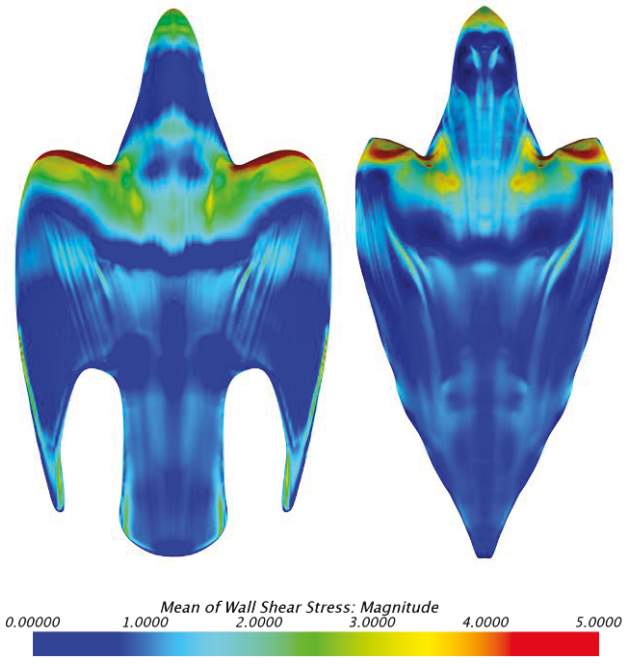

Figure 8. Local wall shear stress distribution obtained from LES for M- and C-shape

the gap between the tail and primary feathers promotes the formation of a strong tail vortex. The presence of vortical structures over tail of birds has been reported previously [7], however the absence of the forebody in that particular experiment raises concerns about how representative the model was with respect to real birds where up- and downstream flow are tightly coupled.

3.2. Evolution of the vortices in the wake

Analyzing the wake data of TR-SPIV and LES, one can immediately identify the strong wing vortices on the outside of both life-size models (see Fig. 9) and the tail vortex in the center region of the M-shaped wing configuration. Interestingly, the channeling of the flow in the gap promotes the formation of other unexpected vortices at the wingtip. When reaching the gap, the flow from the downside starts to curl around the edge induced by the pressure difference between upper and lower side.
The formation of this vortex, called primary feather vortex (PFV), is boosted by the geometry of the wingtip. Due to the natural arrangement of the primary feather in M-shape, the final area of the wingtips shows a geometric discontinuity, similar to a downside facing kink, promoting the roll up of the flow under the wing. Further downstream in the wake, PFV and WV are interacting and roll around each other. For planar wings, an increased lift automatically yields in an increased induced drag theoretically causing the falcon to lose speed. However, the counter-rotating PFV effectively reduces the downwash in the wake and hence, reduces the induced drag. Together with the additional lift from the preconditioned, attached flow the manoeuvrability is greatly increased. These findings explain why a peregrine falcon is often seen to open up its tail and primaries, also during high-speed, allowing it to trim its flight path. This confirms the importance of the M-shape in terms of manoeuvrability during stoop.
As mentioned above, the wake of the C-shape is mainly characterized by the strong wing vortex, as the primaries are stacked on top of the tail feather and thus impede the formation of tail and primary feather vortices. However, the results confirm that the cavity between wing and body promotes an acceleration of the flow on the lower side. The separation line on the body is shifted downstream towards the trailing edge resulting in a reduced form drag of the body [12]. Considering the mentioned live recordings, these findings illustrate that the peregrines falcons effectively use the C-shape to control their speed during dive. Opening up the forearms results in a minor flow acceleration in the cavity and hence, the form drag is increased. If a higher velocity is required during hunt, the wings can be tucked around the body reducing the body drag until the lowest drag configuration, the T-shape, is reached.
The wake studies confirmed the previous assumptions that horn, horseshoe and dorsal vortex are comparatively weak and their influence is localized. However, they have all the same sense of rotation on each side of the body and interact with each other in the dorsal region while propagating further downstream. Thus, the mixing in the inner body part is enhanced and the boundary layer is re-energized. Immediately after reattachment, the flow converges indicating acceleration in the streamwise direction. The effective diameter of the streamtube reduces to a minimum leading to a fully attached and parallel flow when entering the tail feather region. An attached flow over the tail feathers is a major prerequisite to ensure an effective pitch control from the tail. As to avoid uncontrolled deflection or bending from the tail, these feathers are twice as stiff as the ones from other birds [15]. Compared to civil aviation, where the elevators are accounted to be in undisturbed air, peregrine falcons managed to precondition the flow naturally.

.

4. CONCLUSION

From a flight mechanics point of view, the manoeuvrability of peregrine falcons is greatly supported by vortical structures controlling pitch and roll momentum. It appears that these avians have mastered morphology for exceptional aerobatics enabled by an intuitive and natural pre-conditioning of the flow.
Small vortices emanating from the neck and dorsal region and strong spanwise flow enhance mixing and re-energize the local boundary in the inner body region to ensure a quick reattachment and to avoid stall. Thus, a fully attached flow over the tail feathers is achieved for all shapes observed during stoop guaranteeing the effectiveness of the tail feathers as pitch control. These findings are confirmed as the feathers of falco peregrinus are proven to be twice as stiff as those of other birds and hence, are adapted for these high loads.
Spanwise flow and recirculation in the dorsal region are of significant importance for the flight control as the flow related vibrations of the pop-up feather enable peregrine falcons to ‘sense’ the instantaneous flow condition preventing it from stall.
Additional lift generation by suction from stronger vortices similar to those on delta-wings also contribute to the pitching moment, which can be tuned by extending the wing forward and backward.
Keeping M-shape and C-shape during a nose-diving attack requires a robust musculo-skeletal structure, specially to prevent lateral movements of the writs and to maintain the necessary wing position at high-speed.

5. ACKNOWLEDGEMENT

This study was carried out as part of a joint master thesis during the visiting research studentship of CL at City University of London under supervision of Professor Dr.-Ing. habil Christoph Brücker, head of the Sir Richard Olver Chair in Aeronautical Engineering, and RWTH Aachen University under supervision of Professor Dr.-Ing. Wolfgang Schröder, head of the Institute of Aerodynamics and Chair of Fluid Mechanics.
The financial support from City University during this visting research studentship is gratefully acknowledged. The TR-SPIV was supported form the National Wind Tunnel Facility Organization (NWTF). The simulations were run on the Solon Cluster at City University, thanks to the assistance by Chris Marshall. Gratitude is also expressed to the research team involved during the dam test in Hellenthal, Germany. The position of Professor Christoph Brücker is co-funded by BAE SYSTEMS and the Royal Academy of Engineering (Research Chair number RCSFR1617/4/11), which is gratefully acknowledged.

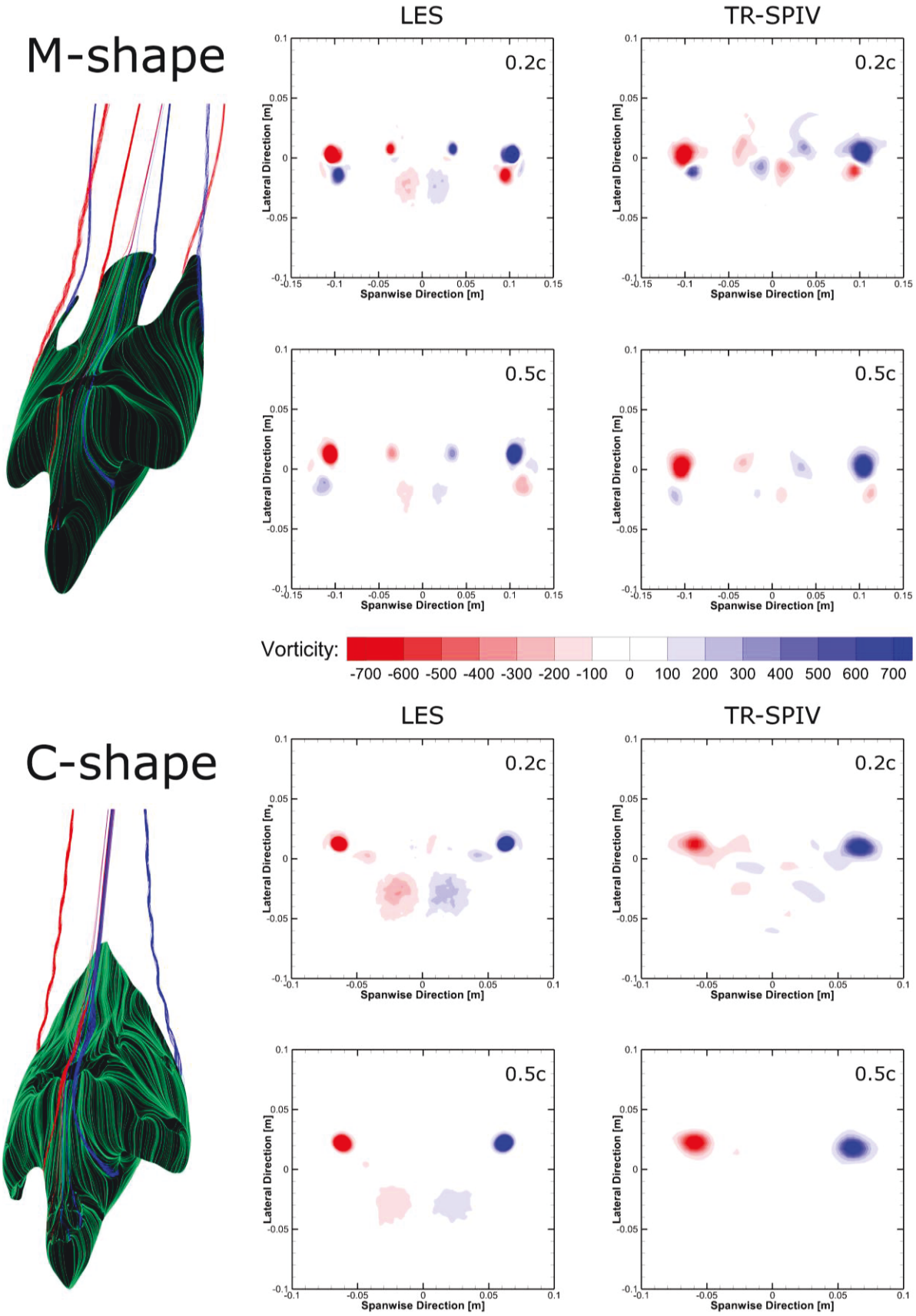

Figure 9. Vorticity distribution in the wake of the M- and C-shape at different measurement planes: Close to the trailing edge (0.2 c), wing, tail and primary feather vortices are visible. With an increasing trailing edge distance, tail and primary feather vortices break down and are barely visible (TR-SPIV data from [5]).

6. REFERENCES

[1] BBC, "Peregrine falcon sky dive – inside the perfect predator, 2010, https://www.youtube.com/watch?v=IegzXQlFNjs.
[2] Birch, M. J., Dickinson, M. H., "Spanwise flow and the attachment of the leading-vortex in insect flight", Nature 421, 729 -733, 2001.
[3] Bjorkquist, D. C., "Stereoscopic PIV calibration verification", 11th International Symposium on Application of Laser Techniques to Fluid Mechanics, Lisbon, Portugal, 2002.
[4] Déléry, J. M., "Robert Legendre and Henri Werlé: toward the eludication of three-dimensional separation", Annu. Rev. Fluid Mech. 33, 129 – 154, 2001.
[5] Gowree, R.E., Jagadeesh, C., Talboys, E., Lagemann, C., Brücker, C., "Vortices enable the complex aerobatics of peregrine falcons", Communcations Biology, 1-27.
[6] Legendre, R., "Separation de l'ecoulement lamnaire tridimensionel", Rech. Aeronaut 54, 3 – 8, 1956.
[7] Maybury, W. J., Rayner, J. M. V., Couldrick, L. B., "Lift generation by the avian tail", Roc. R. Soc. B., 268, 1443 – 1448, 2001.
[8] National Geographic, "High-velocity falcons", 2007, https://video.nationalgeographic.com/video/falcon_peregrine_velocity.
[9] National Geographic, World's deadliest: superfast flyer makes a kill, 2013, https://video.nationalgeographic.com/video/worlds-deadliest/deadliest-peregrine-falcon.
[10] Piomelli, U., "Large-eddy and direct numerical simulations of turbulent flow", von Karman Institute for Fluid Dynamics Lecture Series, 1997.
[11] Poincaré, H. "Les points singuliers des equations différentielles", C. R. Acad. Sci. 95, 416 – 418, 1882.
[12] Ponitz, B., Triep, M., Brücker, C., "Aerodynamics of the Cupped Wings during Peregrine Falcon's Diving Flight", Op. J. Fl. Dyn. 4, 363 – 372, 2014.
[13] Ponitz, B., Schmitz, A., Fischer, D., Bleckmann, H., Brücker, C., "Diving-Flight Aerodynamics of a Peregrine Falcon (Falco Peregrinus), PLoS ONE 9, 1-13, 2014.
[14] Prandtl, L., "Führer durch die Strömungslehre: Grundlagen und Phänomene", Springer Verlag, Berlin, 1931.
[15] Schmitz, A., Ponitz, B., Brücker, C., Schmitz, H., Herweg, J., Bleckmann, H., " Morphological Properties of the Last Primaries, the Tail Feathers, and the Alue of Accipiter nisus, Columba livia, Falco peregrinus and Falco tinnunculus", J. Morphol. 276, 33-46, 2015.
[16] Soloff, S.M., Adrian, R.J., Liu, Z.-C., "Distortion compensation for generalized stereoscopic particle image velocimetry", Meas. Sci. Technol. 8, 1441 – 1454, 1997.
[17] Srygley, R. B., Thomas, A. L. R., "Unconventional lift-generating mechanisms in free-flying butterflies", Nature 420, 660 – 664, 2002.
[18] Tobak, M., Peake, D. J., "Topology of three-dimensional separated flows", Annu. Rev. Fluid Mech. 14, 61 – 85, 1982.
[19] Tucker, V.A., "Gliding flight: speed and acceleration of falcons during diving and pull out", J. exp. Biol. 52, 345 – 367.
[20] Videler, J. J., Stamhuis, E. J., Povel, G. D. E., "Leading-edge vortex lifts swifts", Science 306, 1960 – 1962, 2004.